Rational Construction of a Functionalized V_2O_5 Nanosphere/MWCNT Layer-by-Layer Nanoarchitecture as Cathode for Enhanced Performance of Lithium-Ion Batteries

Bin Sun, Kai Huang, Xiang Qi, Xiaolin Wei, and Jianxin Zhong**

Vanadium pentoxide (V_2O_5) has received considerable attention owing to its potential application in energy storage with high specific capacity (294 mAh g^{-1}). However, the development of V_2O_5 cathodes has been limited by the intrinsically low electrical conductivity and slow electrochemical kinetics resulting in a significant capacity decay. In this article, in order to overcome the issues, V_2O_5 nanospheres and multiwalled carbon nanotubes (MWCNTs) are used to fabricate layer-by-layer composited paper as the cathode, which is prepared via electrostatic interaction and vacuum filtration by alternating the positively charged V_2O_5 nanospheres and the negatively charged terminated MWCNT solutions. As a result, the V_2O_5 nanospheres are closely intercalated between the adjacent MWCNT layers leading to minimize the disadvantage voids and enhance the overall conductivity of the composited electrode, which exhibits an enhanced cycling durability as well as improved rate capability.

1. Introduction

Lithium-ion batteries (LIBs) are used in a wide variety of applications, including portable electronic devices, hybrid electric vehicles (HEVs), and electric vehicles (EVs).[1–8] To meet these constantly increasing demands, the next generation of LIBs requires substantial improvements in energy capacity, cycling stability, and rate capability. Currently, the capacity of cathode electrode is one of the vital limiting factors for the overall cell energy density, and therefore, high capacity cathode materials are extensively studied recently. Among many cathode materials, vanadium pentoxide (V_2O_5) is a promising candidate because of its ease to accommodate molecules or ions into its layered structure. It can accommodate two Li ions with a theoretical capacity of ≈294 mAh g^{-1} when the electrochemical window is in the range of 2–4 V, and possesses certain advantages over the common cathode materials, such as $LiCoO_2$, $LiMn_2O_4$, $LiFePO_4$, etc.[9–13] Moreover, cost effectiveness, facility of synthesis, and abundance in natural resource are other important advantages of investigatingV_2O_5 cathode.

Nevertheless, achieving decent electrochemical performances for V_2O_5 in various aspects, including specific capacity, rate capability, and cycle life, has been a challenge which is ascribed to its low ionic diffusivity and inferior electrical conductivity.[9,14–16] To address these intrinsic drawbacks, an effective strategy was adopted to decrease the active materials to nanoscale level, such as nanowires,[17] nanorods,[18] nanobelts,[19] and nanospheres,[20,21] which can shorten the transport lengths both for electrons and Li ions, minimize the effect of the low ionic diffusivity, and better accommodate the strain of Li ions intercalation/deintercalation in active materials. Moreover, these V_2O_5 nanostructures were also integrated with conductive carbon nanostructures, such as carbon nanotube[22,23] and graphene,[14,24,25] which can not only further enhance the electrical conductivity of V_2O_5 active material, but also help to prevent nanostructured V_2O_5 active materials from agglomeration during cycling. Generally, the electrode is always prepared by mixing together active material, conductive agent, and polymer binder. Due to the nonuniform mixing process, some disadvantage voids can be found in the final prepared electrode, and the active material can easily lose electrical contact with the conductive agent or metal current collector during cycling, resulting in incomplete electrochemical reaction and presenting capacity gradually fading.[26]

Considering these disadvantages, the multiwalled carbon nanotubes (MWCNTs) with good electrical conductivity have been utilized to construct a binder-free layer-by-layer V_2O_5 nanosphere (VOP)/MWCNT nanoarchitecture. In our proposed nanoarchitecture, the VOPs were modified by positive charges and MWCNTs were terminated with negative charges. Then, we have stratified the VOP and MWCNT layers from each other

B. Sun, Prof. K. Huang, X. Qi, X. Wei, Prof. J. X. Zhong
Hunan Key Laboratory for Micro-Nano Energy Materials and Devices
Laboratory for Quantum Engineering and Micro-Nano Energy Technology
School of Physics and Optoelectronics
Xiangtan University
Hunan 411105, P. R. China
E-mail: huangk@xtu.edu.cn; jxzhong@xtu.edu.cn

DOI: 10.1002/adfm.201502382

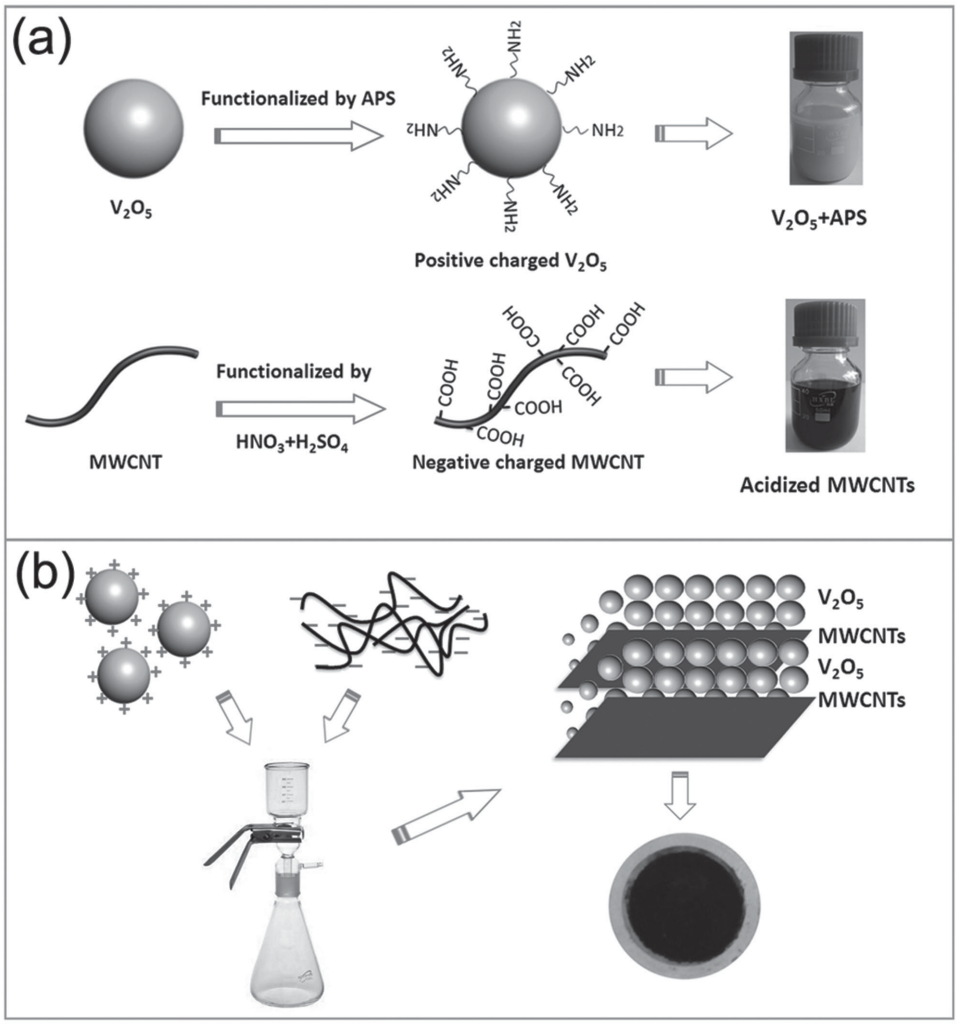

Figure 1. a) Functionalization of the V_2O_5 nanoparticles by grafting APS to render the oxide surface positive charge and acidification of MWCNTs with negative charge, and b) the schematic of constructing the VOP and MWCNT layer-by-layer structures.

via electrostatic interactions and vacuum filtration to obtain a rationally designed multilayer paper, and the detailed process can refer to the Experimental Section (**Figure 1**). This nanoarchitecture can minimize the disadvantage voids between the VOPs and MWCNTs, and enhance the overall conductivity of the final constructed electrode. Moreover, the VOPs were entirely restricted between the MWCNT layers, which can be served as a current collector to avoid the VOPs' losing electrical contact with the conductive MWCNTs during cycling. In addition, the MWCNT layer can also be served as a structural cushion to relax the mechanical stress, and prevent the aggregation of VOPs, and then the structural and electrical integrity of the electrodes are perfectly preserved. More importantly, the lack of a metal current collector, conducting agent, or polymer binder leads to a controllable and improved energy density. Consequently, the heterogeneous nanoarchitecture can be expected to promote electrochemical performance in the rechargeable LIBs with this layer-by-layer VOP/MWCNT paper cathode.

2. Results and Discussion

Upon adding $VO(OiPr)_3$ into a pyridine/acetone/H_2O mixed solution with vigorous stirring in air ambient at room temperature, the as-synthesized product is fine spherical $V_2O_5 \cdot nH_2O$ xerogel with a diameter of ≈200 nm, which can be clearly observed from the scanning electron microscopy (SEM) image in **Figure 2**a. However, some of the water and pyridine molecules were intercalated into V_2O_5 matrix.[27] To remove it, a thermal treatment in air condition was carried out. Then, a smoother and more spherical nanosphere was obtained, which can be seen from the SEM image in Figure 2b. In the meantime, after the annealing process at 350 °C for 3 h, crystalline VOPs can also be obtained. In Figure 2c, the clear diffraction peaks are indexed to the standard orthorhombic V_2O_5 (JCPDF Card No. 77-2418). To further confirm the structure of the product, Raman spectroscopic analysis was employed, depicted in Figure 2d. Two more low-frequency Raman peaks at 195 and 145 cm^{-1} can be distinguished which correspond to the lattice

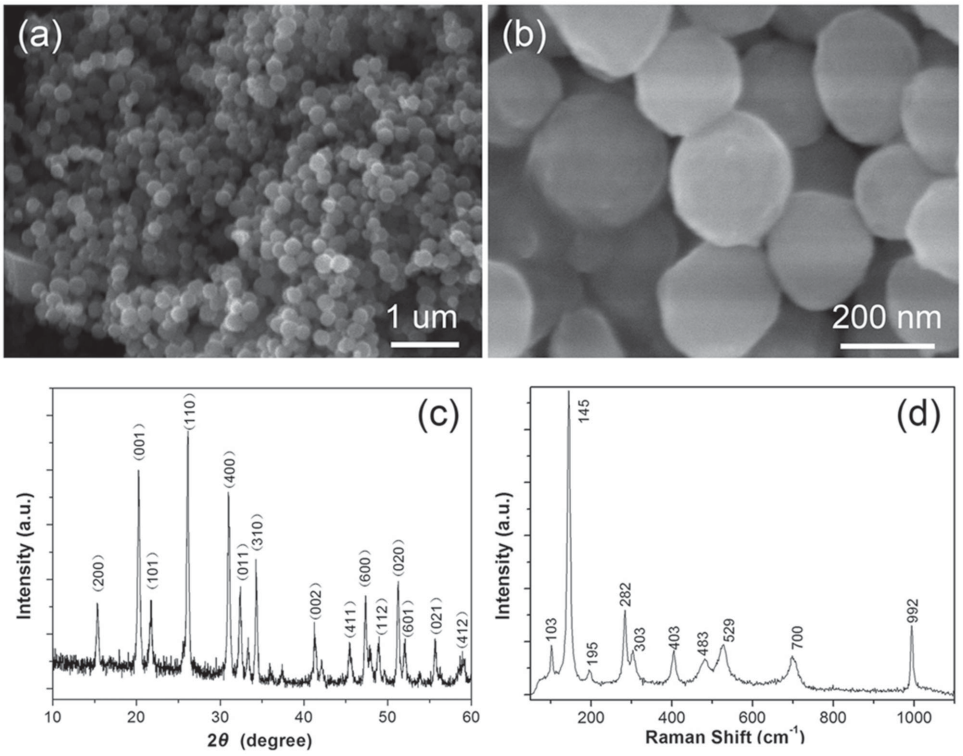

Figure 2. a,b) SEM images of the final obtained V_2O_5 nanospheres with annealing at 350 °C in air condition at different magnification and c) XRD and d) Raman spectrum of the V_2O_5 nanospheres.

vibration, which is strongly associated with the layered structure of V_2O_5.[28,29]

Figure 3 shows the optical images of the final obtained VOP/MWCNT multilayer paper after peeling off from the membrane. Without the functionalization and electrostatic interaction, the VOPs and MWCNTs cannot build a closely multilayer architecture leading to form a disintegrated paper, as shown in Figure 3a. As a stark contrast, the functionalized VOPs and MWCNTs can construct an integrated paper via the electrostatic attraction, after the vacuum filtration process, the composite paper stands as a freestanding paper without using any binder as shown in Figure 3a. As the photograph shows in Figure 3b, the paper can be bent, which implies that the composite paper is mechanically robust, indicating that the paper is applicable as a platform for flexible energy storage devices. All of the results indicate that the electrostatic interaction plays an important role to supply a robust layer-by-layer structure.

To further confirm the unique layer-by-layer architecture of VOP/MWCNT composite, the SEM is employed. In this investigation, as a proof of concept, four typical samples are presented to explicate our designed layer-by-layer architecture. From the cross-sectional SEM images in **Figure 4**a,b, the alternative multilayer structure is obviously and clearly observed, where the VOPs are ideally intercalated between the adjacent MWCNT layers. The six layers of VOPs, with the thickness of each about 2–3 μm, are sandwiched among seven MWCNT layers (≈1 μm), and the overall thickness of the multilayer composite paper is about 20 μm. Due to the electrostatic interactions, more importantly, the positively charged VOP layer can be tightly attached by the negatively charged MWCNT layer. Even through the cutting process by razor-blade for the cross-sectional SEM characterization, no voids can be found between the adjacent layers. The top layer, cross-linked MWCNT network, is fluctuated by the size of VOPs, which can be observed in Figure 4a. In addition, it is worth noting that no VOPs are scattered out and limited beneath the MWCNT layer suggesting

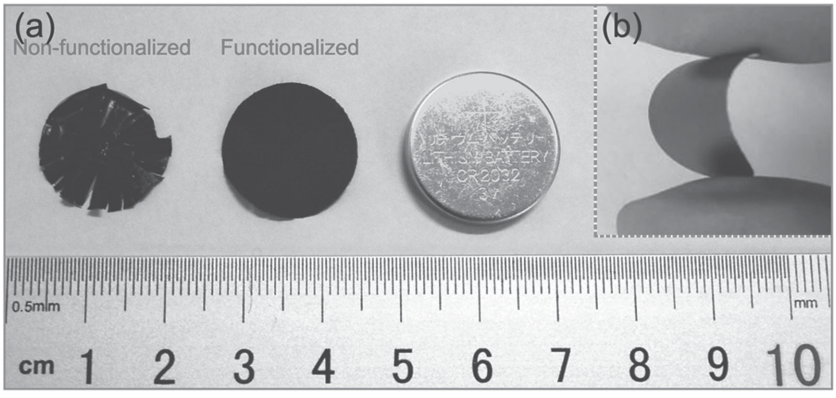

Figure 3. a) A photograph of the functionalized and nonfunctionalized VOP/MWCNT layer-by-layer composite papers; and b) the layer-by-layer composite paper taken under a bent position.

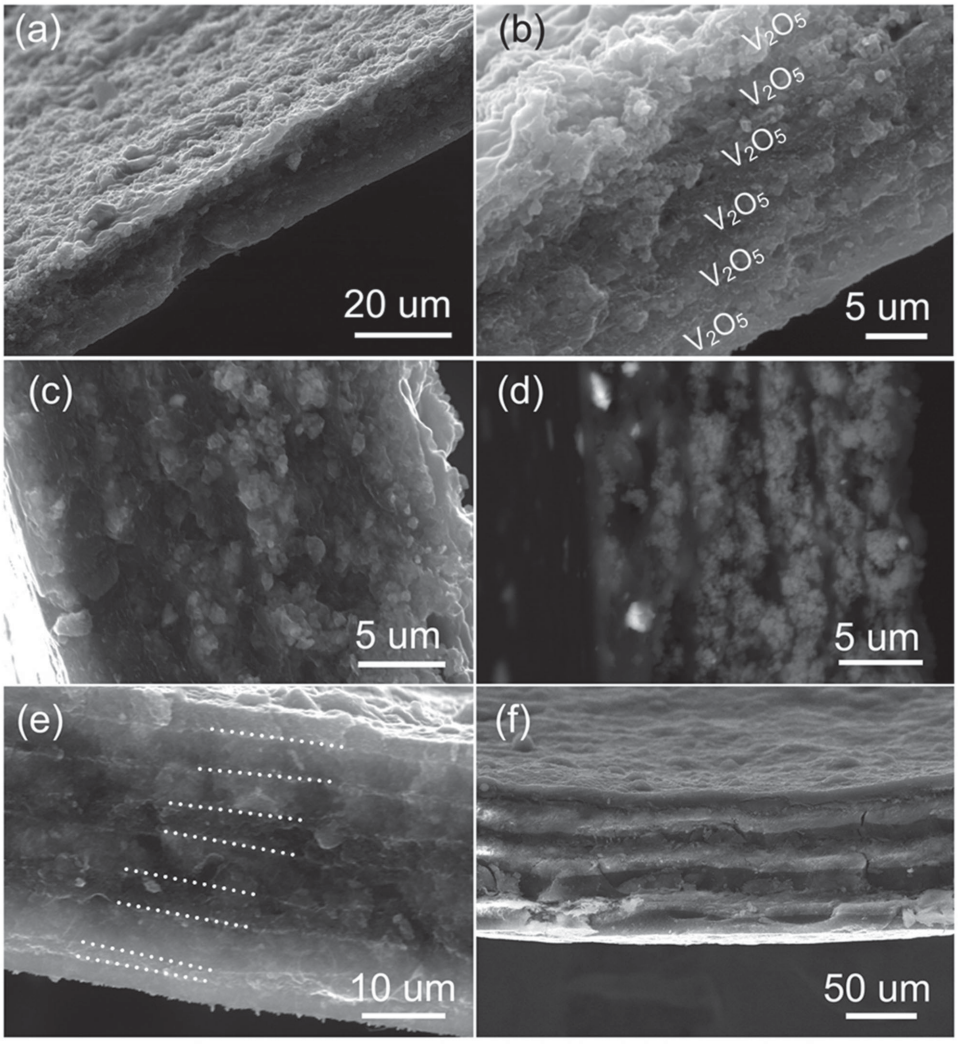

Figure 4. Cross-sectional SEM images of the as-prepared VOP/MWCNT layer-by-layer architecture composites: a,b) five-layer VOPs; c) seven-layer VOPs; d) backscattering SEM image of the composite; and e,f) four layers loading different VOP mass.

the perfect integrity of the obtained VOP/MWCNT layer-by-layer architecture. Figure 4c shows another multilayer composite, and the seven layers of VOPs can be clearly identified from the white areas in Figure 4d, which is a typical backscattering SEM image.

Moreover, bear in mind that the mass loading and the thickness of each VOP and MWCNT layer can be suitably customized and determined by the solution volume added each time or the solution concentration, that is to say, the active mass loading is controllable. As being elucidating this conception, a specific specimen of adjustable VOP layer is also presented. From Figure 4e, we can clearly see that the thickness of VOP stratum changes from 2 to 5 μm, and MWCNT layer is about 2–3 μm, obviously showing that the mass loading can be controlled. It is worth noting that even though the thickness of each loading mass is increased to 10–20 μm, and the overall thickness reaches to ≈100 μm, there is also no obvious voids as shown in Figure 4f. As a result, we have successfully fabricated the rationally designed alternative VOP/MWCNT multilayer composite via electrostatic interaction with integrated architecture.

To understand the electrochemical performances of the layer-by-layer VOP/MWCNT composite paper, a six VOP layer composite has been chosen as the evaluation object. The representative cyclic voltammogram (CV) curves have been measured at a scan rate of 0.2 mV s^{-1} in the voltage range of 2–4 V in **Figure 5**a. The three evident cathodic peaks located at 3.32, 3.10, and 2.15 V indicate the multistep reduction process of V^{+5} in V_2O_5 lattice, and correspond to the phase changes from α-V_2O_5 to ε-$Li_{0.5}V_2O_5$, then δ-LiV_2O_5, and finally γ-$Li_2V_2O_5$, respectively.[30,31] The observed anodic peaks at the potentials of 2.62 and 3.52 V correspond to the Li deintercalation and the successive backward phase transformation. The CV curves are almost identical in the first three cycles, which indicates good reversibility of oxidation/reduction reactions in the electrochemical processes. Figure 5b shows the selected galvanostatic discharge and charge cycles with voltage profiles retaining overlap, which are obtained at a constant current density 0.1 C (1 C is assumed

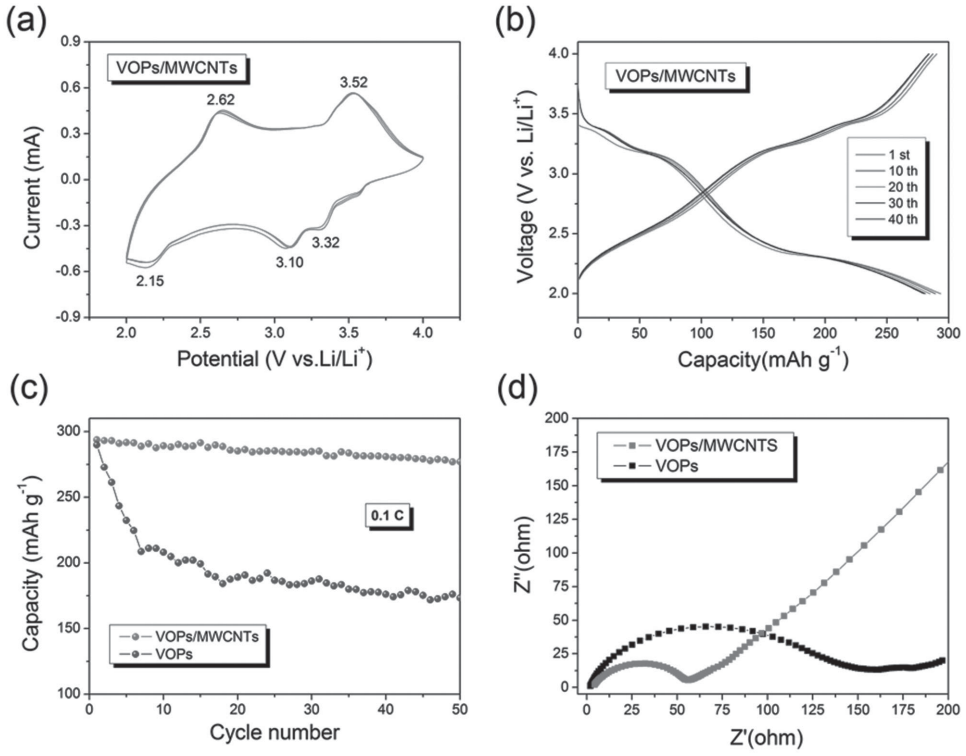

Figure 5. Electrochemical characterizations of the layer-by-layer VOP/MWCNT composite paper. a) The first three CV curves of the composite paper; b) the galvanostatic charge–discharge profiles of the composite; c) the discharge specific capacity of composite and bare V_2O_5 nanospheres at 0.1 C for 50 cycles; and d) Nyquist plots of the layer-by-layer VOP/MWCNT composites and bare VOPs.

to be 294 mA g^{-1}). Consistent with the above CV results, multiple poorly defined voltage plateaus related to the Li ions intercalation and deintercalation are clearly observed. A high specific discharge capacity of 292 mAh g^{-1} can be obtained in the first cycle within a voltage range of 2–4 V. Even for the 50th cycle, a high reversible capacity of 275 mAh g^{-1} can be retained, realizing over 93% of the initial discharge capacity, as shown in Figure 5c, which again indicates the good electrochemical reversibility and extremely stability of the layer-by-layer VOP/MWCNT composite paper. As a comparison, the fading discharge capacity of bare VOPs as shown in Figure 5c (blue curve) exhibits less satisfactory capacity retention, and the capacity quickly dropped down to 160 mAh g^{-1} after 50 cycles.

Furthermore, to further elucidate the electrochemical performance of layer-by-layer VOP/MWCNT composite and bare VOPs, respectively, electrochemical impedance spectroscopy (EIS) was carried out and presented in Figure 5d. EIS is a simple and versatile technique to understand the electrochemical reactions occurring within the cells. The high-to-middle frequency semicircle can be observed which is related to the formation of solid electrolyte interphase (SEI) layer and surface paper capacitance, while the middle-to-low frequency region refers to the charge transfer (CT) and interfacial capacitance across the electrode–electrolyte interface. The inclined vertical line at 45° in low-frequency regions refers to the lithium diffusion–related kinetics.[32,33] It is clearly observed that the diameter of the semicircles showed a further smaller value with the layer-by-layer architecture than that of bare VOPs, which arises from the outstanding electron transport capability of active material and ionic conductivity of the electrolyte filled in the pores of composite electrode. And it was well reflected in our electrochemical cycling studies.

Taking into account the effect from layer numbers of VOPs, the high cycling stability and rate capability of the six-layer (as shown in Figure 4b) and four-layer VOPs (as shown in Figure 4e) are further demonstrated in **Figure 6**. Reversibility of the storage capacity of both samples were observed when the rate was first increased stepwise from 0.2 to 4 C, and then switched back to 0.2 C, as shown in Figure 6a. When the current density is up to 4 C, the discharge capacity of composite can be stabilized at 130 mAh g^{-1}, which demonstrates facile Li intercalation/deintercalation in the active material. When cycled at 1 C, we can see the perfect stability of the two designed composites, the capacity of which is about 200 mAh g^{-1} in the 100th cycle in Figure 6b.

The high stability and good rate capability of the both samples reveal that the active VOPs, restrainedly confined among either seven or five MWCNT layers, can sufficiently participate in the lithiation and delithiation cycles. This is believed to contribute to the close resembling electrochemical performance of our two designed composites. The results further highlight the essential element of the cathode materials, and that all of the active materials are serviceable and functional.

Apart from that, the thickness effect of the layer should also be taken into consideration. The cycling performances of the two samples, both of which possess four VOP layers with different gross thickness in Figure 4e (30 μm) and Figure 4f

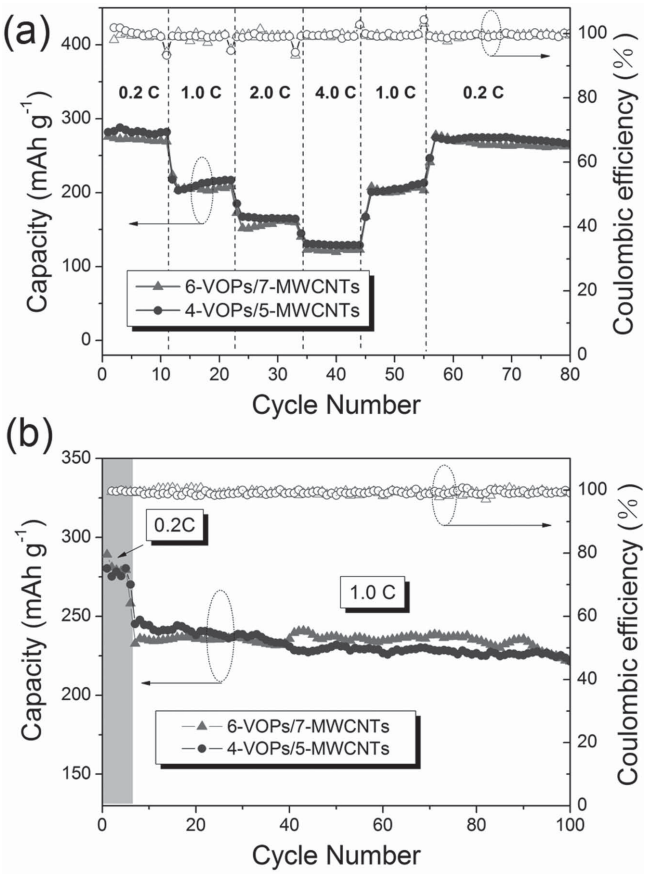

Figure 6. a) The as-prepared six layers and four layers of VOP composites at current densities of 0.2, 1, 2, and 4 C, and then switched back to 0.2 C and b) capacity–cycle profiles of the two composites for 100 cycles at 1 C.

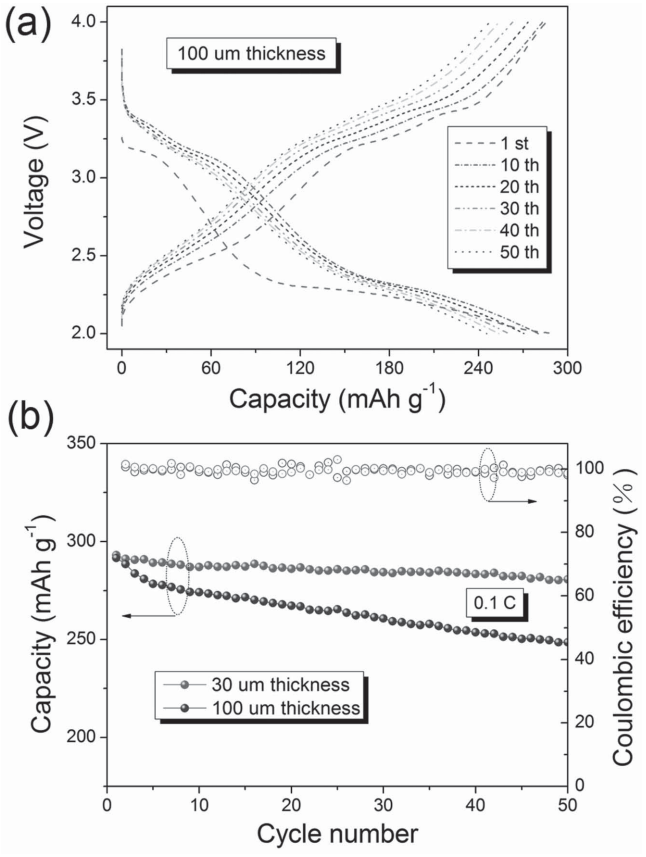

Figure 7. a) The galvanostatic charge–discharge profiles of the composite with 100 μm thickness and b) the discharge specific capacity of the two composites with 30 and 100 μm thickness at 0.1 C for 50 cycles, respectively.

(≈100 μm), were evaluated at 0.1 C rate, as shown in **Figure 7**. The clearly fading phenomena of the thicker sample with single VOP layer about 15 μm can be observed, and the capacity decreases from the initial 288 to 250 mAh g^{-1} after 50 cycles. However, for the thinner sample with single VOP layer about 2–5 μm, no obvious capacity decline or tendency of capacity decay can be seen. This is believed to result from the thickness of the single VOP layer. With the VOP layer thickness increasing, it is inevitable that the conductivity of the overall electrode can be disappointing. Especially, when the thickness of the VOP layer reaches to 10 or 20 μm, the conductivity of VOPs in the middle of layer should be seriously reduced, resulting in the slight capacity fading with long time cycling. In addition, the MWCNT layers only serve as the conductive layer, and the porous MWCNT layer is available to the penetration of liquid electrolyte. And that, the change of the thickness of MWCNT layers cannot attribute to the capacity decline.

3. Conclusions

A novel architecture of layer-by-layer VOPs/MWCNTs has been successfully prepared through an efficient electrostatic interaction. The obtained flexible layer-by-layer composite exhibits an enhanced reversible capacity and improved cycling characteristic, even under the current density of 1 C, the composited paper is capable of retaining a specific capacity of 200 mAh g^{-1} over 100 cycles. The excellent electrochemical performance of such composite might be related to the tightly attached unique layer-by-layer architecture in several aspects. First, the MWCNT layer, sandwiched between two VOP layers, can be served as an excellent conductive layer for the adjacent upper and lower VOP layers. Especially, the VOP layers and MWCNT layers construct a closely contacted architecture via electrostatic interaction. Even pulverization during cycling, the VOPs are still restricted in the adjacent MWCNT layers keeping closely in contact with the conductive MWCNT layer. Second, the small gaps from the MWCNT network and the VOPs ensure efficient electrolyte penetration and increase the contact area between the electrode and electrolyte. Furthermore, the layer-by-layer architecture would effectively block the aggregation of the VOPs. Finally, the flexible MWCNT layer can also accommodate the strain of Li intercalation/deintercalation in V_2O_5 matrix. Furthermore, the scalable layer-by-layer structure can be readily applied to other lithium-ion batteries which suffer from dramatic volume expansion or low intrinsic electric conductivity.

4. Experimental Section

Materials Synthesis and Characterization: VOPs were synthesized from vanadium isoporpoxide ($VO(OiPr)_3$, Sigma-Aldrich) through hydrolysis.[27,34] A typical process is as follows: deionized water (0.1 mL), acetone (90 mL), and pyridine (4 mL) were mixed together in a big container to form a homogeneous solution, and the mixed solution was vigorously stirred for 10 min. Then, $VO(OiPr)_3$ (0.4 mL) was added into the above solution, and the color of solution immediately turned into milky orange. The hydrolyzate was obtained by centrifugal separation, and washed by acetone for three times. The final product was annealed at 350 °C for 3 h in ambient air.

In order to positively charge the oxide surface, VOPs were modified by surface grafting of aminopropyltrimethoxysilane (APS, Sinopharm),[35] as shown in Figure 1a. Briefly, VOPs (0.1 g) and APS (0.1 mL) were dissolved in toluene (10 mL), then the mixed solution was ultrasonicated for 30 min. After centrifugation, the obtained product was further dried in vacuum oven at 60 °C for 5 h. The MWCNTs (commercial product) were negatively charged by functionalizing with concentrated nitric acid and sulfuric acid (HNO_3/H_2SO_4, 1:3 volume ratio) as shown in Figure 1b.[36] Finally, 9 mg modified VOPs were uniformly dispersed into deionized water (40 mL) by ultrasonication for 1 h (yellow bottle), and so do for the functionalized MWCNTs (1 mg, black bottle). With vacuum filtration treatment, the composited multilayer paper was obtained alternately with the two solutions, as shown in Figure 1b.

Material and Electrode Characterization: The structure and morphology of the samples were characterized by scanning electron microscopy (FESEM, Hitachi S-4800), micro-Raman spectroscope (WITec excited by $\lambda = 633$ nm laser), and X-ray powder diffraction (XRD, D/MAX 2500).

To evaluate the electrochemical performance of the cathode, the obtained V_2O_5/MWCNT composite paper was cut into desired size and assembled into 2032-type coin cells in which Celgard 2400 and Li foil were used as separators and counter/reference electrodes, respectively. It is worth noting that there is no capacity contribution from MWCNTs at the potential window 2–4 V, so, we have only calculated the mass of the VOPs. The electrolyte used was lithium hexafluorophosphate (1 M, $LiPF_6$), dissolved in 1/1/1 (volume rate) ethylene carbonate (EC)/ethyl methyl carbonate (EMC)/diethyl carbonate (DMC). Particularly, the cells were assembled in an argon-filled glove box. CV curves were achieved with an electrochemistry system (CHI 660D, China). The constant current charge and discharge measurements in a voltage range between 2 and 4 V (vs Li/Li^+) were conducted using Neware Technology (NEWARE BTS-5V 5 mA, Neware Technology Co, Ltd., China).

Acknowledgements

The authors would like to acknowledge financial supports provided by innovation platform of Hunan colleges (No. 14K090), National Natural Science Foundation of China (No. 51172191), and Changjiang Scholars and Innovative Research Team in University (IRT13093).

Received: June 11, 2015
Revised: June 28, 2015
Published online: August 4, 2015

[1] X. Li, J. H. Cho, N. Li, Y. Zhang, D. Williams, S. A. Dayeh, S. T. Picraux, *Adv. Energy Mater.* **2012**, *2*, 87.
[2] M. Armand, J. M. Tarascon, *Nature* **2008**, *451*, 652.
[3] F. Sun, K. Huang, X. Qi, T. Gao, Y. Liu, X. Zou, X. Wei, J. X. Zhong, *Nanoscale* **2013**, *5*, 8586.
[4] Y. Liu, K. Huang, Y. Fan, Q. Zhang, F. Sun, T. Gao, L. Yang, J. Zhong, *Electrochim. Acta* **2013**, *88*, 766.
[5] Y. P. Liu, K. Huang, Y. Fan, Q. Zhang, F. Sun, T. Gao, Z. W. Wang, J. X. Zhong, *Electrochim. Acta* **2013**, *102*, 246.
[6] J. Zhu, L. Chen, Z. Xu, *Nano Energy* **2015**, *12*, 339.
[7] J. Zhu, Z. Xu, B. Lu, *Nano Energy* **2014**, *7*, 114.
[8] C. Wang, L. X. Wu, H. Wang, W. H. Zuo, Y. Y. Li, J. P. Liu, *Adv. Funct. Mater.* **2015**, *25*, 3524.
[9] Y. Li, J. Yao, E. Uchaker, J. Yang, Y. Huang, M. Zhang, G. Cao, *Adv. Energy Mater.* **2013**, *3*, 1171.
[10] S. Luo, K. Wang, J. Wang, K. Jiang, Q. Li, S. Fan, *Adv. Mater.* **2012**, *24*, 2294.
[11] X. Xiao, J. Lu, Y. Li, *Nano Res.* **2010**, *3*, 733.
[12] L. Wang, W. Sun, X. Tang, X. Huang, X. He, J. Li, Q. Zhang, J. Gao, G. Tian, S. Fan, *J. Power Sources* **2013**, *244*, 94.
[13] S. T. Myung, M. H. Lee, S. Komaba, N. Kumagai, Y. K. Sun, *Electrochim. Acta* **2005**, *50*, 4800.
[14] J. W. Lee, S. Y. Lim, H. M. Jeong, T. H. Hwang, J. K. Kang, J. W. Choi, *Energy Environ. Sci.* **2012**, *5*, 9889.
[15] Y. L. Cheah, R. Hagen, V. Aravindan, R. Fiz, S. Mathur, S. Madhavi, *Nano Energy* **2013**, *2*, 57.
[16] E. Potiron, A. L. G. A. Salle, A. Verbaere, Y. Piffard, D. Guyomard, *Electrochim. Acta* **1999**, *45*, 197.
[17] L. Q. Mai, L. Xu, C. Han, X. Xu, Y. Luo, S. Zhao, Y. Zhao, *Nano Lett.* **2010**, *10*, 4750.
[18] K. Takahashi, S. J. Limmer, Y. Wang, G. Cao, *J. Phys. Chem. B* **2004**, *108*, 9795.
[19] D. Chao, X. Xia, J. Liu, Z. Fan, C. F. Ng, J. Lin, H. Zhang, Z. Shen, H. J. Fan, *Adv. Mater.* **2014**, *26*, 5794.
[20] T. Kim, J. Shin, T. S. You, H. k. Lee, J. Kim, *Electrochim. Acta* **2015**, *164*, 227.
[21] A. Q. Pan, H. B. Wu, L. Yu, X. W. Lou, *Angew. Chem., Int. Ed.* **2013**, *52*, 2226.
[22] M. Sathiya, A. S. Prakash, K. Ramesha, J. M. Tarasconand, A. K. Shukla, *J. Am. Chem. Soc.* **2011**, *133*, 16291.
[23] X. Jia, L. Zhang, R. Zhang, Y. Lu, F. Wei, *RSC Adv.* **2014**, *4*, 21018.
[24] Z. F. Li, H. Zhang, Q. Liu, Y. Liu, L. Stanciu, J. Xie, *ACS Appl. Mater. Interfaces* **2014**, *6*, 18894.
[25] J. Cheng, B. Wang, H. L. Xin, G. Yang, H. Cai, F. Nie, H. Huang, *J. Mater. Chem. A* **2013**, *1*, 10814.
[26] J. N. Weker, N. Liu, S. Misra, J. C. Andrews, Y. Cui, M. F. Toney, *Energy Environ. Sci.* **2014**, *7*, 2771.
[27] S. Wang, Z. Lu, D. Wang, C. Li, C. Chen, Y. Yin, *J. Mater. Chem.* **2011**, *21*, 6365.
[28] S. H. Lee, H. M. Cheong, M. J. Seong, P. Liu, C. E. Tracy, A. Mascarenhas, J. R. Pitts, S. K. Deb, *J. Appl. Phys.* **2002**, *92*, 1893.
[29] R. B. Smirnov, K. S. Smirnov, V. Y. Kazimirov, J. M. G. Amores, U. Amador, M. E. A. Dompablo, J. P. Pereira-Ramos, *Inorg. Chem.* **2012**, *51*, 3194.
[30] Y. L. Cheah, N. Gupta, S. S. Pramana, V. Ravindan, G. Wee, M. Rinivasan, *J. Power Sources* **2011**, *196*, 6465.
[31] Y. L. Cheah, V. Aravindan, S. Madhavi, *J. Electrochem. Soc.* **2013**, *160*, A1016.
[32] V. Aravindan, K. Karthikeyan, K. S. Kang, W. S. Yoon, W. S. Kimf, Y. S. Lee, *J. Mater. Chem.* **2011**, *21*, 2470.
[33] Y. Liu, K. Huang, H. Luo, H. Li, X. Qi, J. Zhong, *RSC Adv.* **2014**, *4*, 17653.
[34] S. Yamamotoa, M. Takanoa, Y. Shimakawa, *MRS Proc.* **2005**, *27*, 879.
[35] S. Yang, X. Feng, S. Ivanovici, K. Müllen, *Angew. Chem., Int. Ed.* **2010**, *49*, 8408.
[36] S. W. Lee, N. Yabuuchi, B. M. Gallant, S. Chen, B. S. Kim, P. T. Hammond, Y. S. Horn, *Nat. Nanotechnol.* **2010**, *5*, 531.